Progress In Electromagnetics Research C, Vol. 106, 121–136, 2020

Optimal Design Methodology for Planar Multi-Layered Radomes for Multiband Applications Using Nature Inspired Algorithm

Vineetha Joy[1, *], Ambika J. Teena[2], Hema Singh[1], and Raveendranath U. Nair[1]

Abstract—An efficient nature inspired algorithm based on particle swarm optimization (PSO) is presented in this paper for the optimal design of planar multi-layered radomes for multiband applications. Material layer sequence and thickness profile are the two critical factors determining the position of passbands in the frequency range of operation as well as the transmission performance in those bands. These design aspects have to be appropriately optimized to achieve the desired performance, and it becomes a daunting task for radome designers when a comparatively large database of suitable materials is available in the solution space. Even though commercially available software packages provide options (like particle swarm optimization (PSO), genetic algorithm (GA), etc.) for the optimization of thickness profile, they do not have the functionality for optimizing the position of a specific material inside the multi-layered radome wall configuration. In this regard, the proposed PSO-based algorithm automatically chooses suitable materials from the predefined database and optimizes the thickness for each layer, in order to achieve superior transmission in user defined passbands. Furthermore, the superiority of the indigenously developed algorithm over the optimization techniques available in full wave simulation software (FEKO) w.r.t. accuracy and computational efficiency is also established using suitable case studies and validations. Although PSO has been used in the context of radomes, its application for the simultaneous optimization of material layer sequence and thickness profile of multi-layered radomes is not reported in literature to the best of our knowledge.

1. INTRODUCTION

Radomes are critical structures used to protect sensitive antennas from harsh environmental conditions without degrading their electromagnetic performance. With respect to aerospace domain, various antennas are mounted on aircrafts/missiles for different applications like navigation, communication, surveillance, and detection. However, these antennas are frequently exposed to severe physical conditions like wind, snow, rain, bird impacts, lightning strikes, hailstorms, extreme temperature gradients, etc. Therefore, an electromagnetically efficient and structurally stable radome is an essential prerequisite for such antennas. Furthermore, radar systems are becoming more autonomous to simultaneously detect various multiple targets at different frequencies and at the same time diffuse all possible countermeasure strategies. These state of the art systems therefore should have seeker units capable of operating at multiple frequency bands which in turn need multi-band antennas. This requirement automatically calls out for the development of multi-band radomes with superior transmission performance in predefined bands. The objective to achieve superior transmission in multiple bands will be a difficult task with the design of a streamlined radome being a complex problem even for single frequency applications.

Several radome wall configurations have been reported in literature for multiband applications [1–6]. Zhou et al. proposed an A-sandwich radome for dual-band applications where each layer was designed with a thickness of (1/12)th wavelength corresponding to a particular design frequency [1]. Later, they

Received 30 June 2020, Accepted 29 September 2020, Scheduled 14 October 2020
* Corresponding author: Vineetha Joy (vineethajoy@nal.res.in).
[1] Centre for Electromagnetics (CEM), CSIR-National Aerospace Laboratories, Kodihalli, Bangalore-560017, India. [2] Cochin University of Science and Technology, Kochi, India.

laid out a method for tackling this specific design problem with odd number of layers [2]. Further, Zhou et al. suggested a flat multilayer radome wall structure with passbands positioned at odd multiples of chosen central frequencies [3] and a graded porous structure for high-temperature applications [4]. Another contribution regarding dual-band configuration has been from Pei et al. where alternating layers of staggered composite and Kagome lattice structures were used [5]. Silicon nitride based graded porous radome models for broadband and dual-band high Mach applications have also been reported in [6] and [7], respectively.

Apart from multi-layered radome wall configurations composed of homogenous material layers, frequency selective surface (FSS) based radomes present another attractive option for the realization of multi-band functionality. Xu et al. presented a computationally efficient technique for the design and optimization of multi-layered FSSs for realizing multiple stopbands [8, 9]. Here, several layers with dog bone shaped patches optimized for specific stopband responses have been cascaded together to generate the multiband response. Dual-band response with independent control over the operational frequency range has been achieved in [10] using multiple dielectric layers containing periodic arrays of inductive wire grids and capacitive patches. In a similar manner, a dual band FSS based multi-layered radome has been presented in [11] with two passbands operating at 10 GHz and 14 GHz, respectively. Further, Yan et al. [12] proposed a three layered FSS based configuration using double square loops and gridded-double square loops for realizing three transmission bands centred at 7.7 GHz, 12.8 GHz, and 18.9 GHz. Although FSSs are highly functional for realizing multiple transmission bands, an inherent disadvantage of such radome models is the degradation in radiation performance due to mutual coupling between antenna and FSS elements. Furthermore, it is difficult to obtain an FSS based design which is insensitive to variations in angle of incidence and polarization of electromagnetic signals. In addition, the fabrication of FSS-based non-planar radomes with gradually varying unit cell dimensions, periodicity, etc. is indeed a major challenge.

The inability of conventional radome wall configurations in achieving multi-band capabilities with randomly located passbands and the practical difficulties associated with FSS based radomes are clearly evident from the above mentioned reported works. Multi-layered radome wall models with distinctly tailored material layer sequence and thickness profile present an excellent choice in this regard. More specifically, functionally graded material (FGM) based radomes, where the properties of base material are intelligently varied to achieve the required gradation in permittivity, are highly attractive especially for high Mach applications [4, 6, 7]. FGMs were introduced in early 1990s with the aim to reduce the thermal stress between consecutive layers which was a major issue for reentry vehicles that undergo ultra-high temperature gradients [13, 14]. Radome wall configurations made up of dissimilar materials get easily destroyed under such conditions due to the difference in thermal expansion coefficients of constituent materials at junctions. This kind of high levels of stress at junctions can cause delamination or cracks. This inherent drawback is applicable to conventional sandwich radomes as well as multi-layered radomes made up of entirely different base materials. On the other hand, since base material is the same across FGM based radome wall, the induced thermal stress in high temperature environments will be less.

With respect to multi-layered radomes, material layer sequence and thickness profile are the two critical factors determining the position of passbands in the frequency range of operation as well as the transmission performance in those bands. However, the optimization of these parameters becomes computationally intensive especially when a huge database of potential materials is available. In this regard, an efficient particle swarm optimization (PSO) based algorithm for material selection as well as thickness optimization of multi-layered planar radomes for multi-band applications is presented in this paper. PSO has been found to be very efficient in dealing with multi-dimensional multi-objective problems with considerably reduced computational complexity. One of the advantages of PSO compared to other nature inspired algorithms like differential evolution, genetic algorithm (GA), central force algorithm, etc. is its simplicity, and PSO in certain instances has outperformed other techniques like GA [15]. With reference to electromagnetic problems with multiple dielectric layers, PSO has been successfully used for the optimization of multi-layered radar absorbing structures [16, 17]. Chiba et al. [18] used PSO to optimize the thickness profile and shape of a seven-layered sandwich radome with pre-identified material layer sequence. On an identical note, the optimization of thickness as well as permittivity profile of a C-sandwich radome has been attempted using PSO in [19]. Further, Nguyen

et al. [20] used PSO as well as ant colony optimization algorithm for obtaining the thickness profile of a C-sandwich radome. However, the application of PSO for the simultaneous optimization of material layer sequence and thickness profile of multi-layered radomes is not reported in literature to the best of our knowledge.

In this paper, an indigenously developed PSO based algorithm is presented to automatically identify the optimal material layer sequence and thickness profile for a multi-layered radome with multi-band functionality, given a predefined material database and range of possible thicknesses. The fitness function has been uniquely formulated so that the predicted radome wall configuration provides maximum power transmission and minimum power reflection in the user-defined passbands for a comparatively high angle of incidence. In order to improve the accuracy of the optimization algorithm, a full wave formulation [21] has been used for the computation of overall reflection/transmission coefficients of the multi-layered radome. Further, insertion phase delay (IPD), a critical factor contributing to bore-sight error (BSE), is also computed for the predicted multi-layered radome wall configuration.

2. PROPAGATION OF ELECTROMAGNETIC WAVES IN MULTI-LAYERED RADOMES

Planar multi-layered radomes consist of a number of material layers stacked one over another following a particular sequence. This arrangement results in interfaces at which the constitutive parameters change abruptly. These discontinuities give rise to intermediate boundaries at which reflection and transmission occur. Consider such a planar multi-layered radome with M layers, as shown in Fig. 1. The entire structure can be considered as an inhomogeneous medium where the constitutive parameters are constant in each layer. Further, the layers are assumed to extend infinitely along X and Y directions. The thickness, complex permittivity, and complex permeability of mth layer are denoted by t_m, $\varepsilon_m = \varepsilon'_m - \varepsilon''_m$, and $\mu_m = \mu'_m - j\mu''_m$, respectively. The series of multiple reflections and transmissions occurring across the interfaces, for a plane wave incident obliquely on the multi-layered radome, is clearly illustrated in Fig. 1. Here, it is evident that the overall reflection from a particular layer includes the effect of reflections from all the layers beneath it.

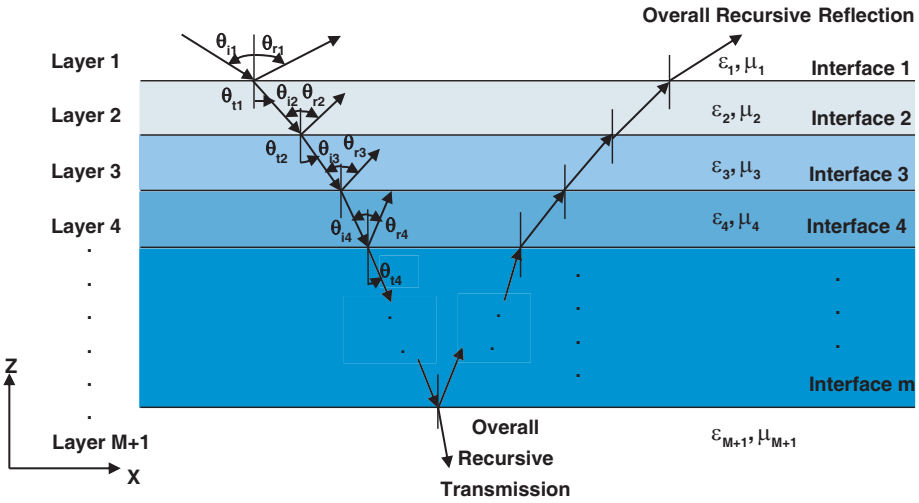

Figure 1. Series of multiple reflections and transmissions occurring in a multi-layered radome wall configuration.

3. COMPUTATION OF OVERALL RECURSIVE COEFFICIENTS

In order to compute the overall recursive reflection and transmission coefficients corresponding to a multi-layered radome wall configuration, the intrinsic (or Fresnel) coefficients need to be calculated at

each and every interface. This in turn involves the computation of angle of incidence at each interface using Snell's law of refraction.

The Fresnel reflection (RC_{TE}) and transmission (TC_{TE}) coefficients at the interface between Layer#m and Layer#$(m+1)$ for TE polarized plane waves can be written as [21–23],

$$RC_{TE_{m,m+1}} = \frac{\eta_{m+1}\cos\theta_{im} - \eta_m \cos\theta_{tm}}{\eta_{m+1}\cos\theta_{im} + \eta_m \cos\theta_{tm}} \tag{1}$$

$$TC_{TE_{m,m+1}} = \frac{2\eta_{m+1}\cos\theta_{im}}{\eta_{m+1}\cos\theta_{im} + \eta_m \cos\theta_{tm}} \tag{2}$$

where η_m and η_{m+1} denote the wave impedances corresponding to the mth and $(m+1)$th layer, respectively. θ_{im} and θ_{tm} are the angles made by incident ray and refracted ray, respectively, with the normal to the interface.

Similarly, the Fresnel reflection (RC_{TM}) and transmission (TC_{TM}) coefficients corresponding to TM polarized plane waves can be written as [21–23],

$$RC_{TM_{m,m+1}} = \frac{\eta_{m+1}\cos\theta_{tm} - \eta_m \cos\theta_{im}}{\eta_{m+1}\cos\theta_{tm} + \eta_m \cos\theta_{im}} \tag{3}$$

$$TC_{TM_{m,m+1}} = \frac{2\eta_{m+1}\cos\theta_{tm}}{\eta_{m+1}\cos\theta_{tm} + \eta_m \cos\theta_{im}} \tag{4}$$

Once the intrinsic reflection/transmission coefficients corresponding to respective polarizations are computed for all the interfaces, the recursive reflection coefficient ($\widetilde{RC}_{m,m+1}$) at the interface between Layer#m and Layer#$(m+1)$ can be defined as [21–23],

$$\widetilde{RC}_{m,m+1} = \frac{RC_{m,m+1} + \left(\widetilde{RC}_{m+1,m+2}\right) \times q}{1 + \left(RC_{m,m+1}\,\widetilde{RC}_{m+1,m+2}\right) \times q} \tag{5}$$

where $q = e^{2jk_{(m+1)z}(d_{m+1}-d_m)\cos\theta_{tm}}$, d_m and d_{m+1} denote the thickness of Layer#m and Layer#$(m+1)$, respectively. The equation clearly indicates that the recursive reflection at mth layer corresponds to the overall reflection from mth layer including the reflections from all the layers present beneath it. In the present case, $\widetilde{RC}_{1,2}$ will denote the overall recursive reflection coefficient corresponding to the multilayered radome wall. Moving further, the overall recursive transmission coefficient ($\widetilde{TC}_{1M}$) for the multi-layered radome can be expressed as [21–23],

$$\widetilde{TC}_{1M} = \prod_{m=1}^{M-1} e^{j\,k_{m\,z}(d_m - d_{m-1})\cos\theta_{t(m-1)}} S_{m,m+1} \tag{6}$$

where,

$$S_{m,m+1} = \frac{1 + RC_{m,m+1}}{1 + RC_{m,m+1}\widetilde{RC}_{m+1,m+2} \times q} \tag{7}$$

Depending upon the polarization of the incident plane wave, the corresponding Fresnel coefficients, as presented in Equations (1) through (4) have to be appropriately substituted in Equations (5) through (7).

Another critical parameter which plays a major role in determining the bore-sight error (BSE) induced by radomes is insertion phase delay (IPD). It is particularly important for fire control radars where a slight change in direction can be disastrous. IPD basically includes the phase difference between the incident wave and transmitted wave as well as the phase difference due to the path difference occurring as a result of refraction in each layer [24–26].

The overall recursive transmission coefficient ($\widetilde{TC}_{1M}$) of the multi-layered radome wall can be expressed as,

$$\widetilde{TC}_{1M} = \widetilde{TC}_{1M_{real}} + j\widetilde{TC}_{1M_{imag}} \tag{8}$$

Therefore, the phase difference between incident wave and transmitted wave can be written as,

$$-\angle\widetilde{TC}_{1M} = \tan^{-1}\left(\frac{-\widetilde{TC}_{1M_{imag}}}{\widetilde{TC}_{1M_{real}}}\right) \tag{9}$$

Further, the phase difference due to the path difference introduced as a result of refraction through M layers can be written as,

$$\phi = t_1\cos\theta_1 + t_2\cos\theta_2 + \ldots + t_m\cos\theta_m + \ldots + t_M\cos\theta_M \tag{10}$$

where t_m and θ_m denote the thickness of the mth layer and the angle of incidence in mth layer, respectively. Therefore, the total insertion phase delay (IPD) can be expressed as [24–26],

$$IPD = -\angle\widetilde{TC}_{1M} - \frac{2\pi}{\lambda}\phi \tag{11}$$

4. PARTICLE SWARM OPTIMIZATION (PSO) IN THE CONTEXT OF DESIGN OF MULTI-LAYERED RADOMES

Particle swarm optimization (PSO), a computationally brilliant swarm intelligence-based algorithm, presents a suitable choice for the optimization of material layer sequence and thickness profile of multi-layered radome wall configurations for multi-band applications. PSO has been found to be very efficient in dealing with multi-dimensional multi-objective problems with considerably reduced computational complexity and high ease of implementation in comparison with other nature inspired algorithms like differential evolution, genetic algorithm (GA), central force algorithm, etc.

PSO draws analogy from the movement of a swarm of bees where the position of each bee corresponds to a possible solution to the problem [27]. The important terms that will be encountered during the implementation of PSO based algorithm, in the context of design and optimization of multi-layered radome wall configurations, are explained below:

(i) *Particle*: An individual bee from the swarm is referred to as a particle.

(ii) *Position*: With respect to the swarm of bees moving in search of flowers, position corresponds to the particular location of a bee in the garden. Correlating to real time problems, each position corresponds to a potential solution to the task at hand which in turn refers to the set of parameters to be optimized. In the case of optimization of multi-layered radome wall configuration, the position of each particle would be a set of materials and the corresponding thicknesses.

(iii) *Fitness function*: The quality of a particular position is evaluated with the help of fitness function. The set of parameters constituting the position of a particular particle will be taken as input to the fitness function and a value representing the degree of goodness of that position will be returned back as output. In the present case, a position can be considered good, if the radome wall made up of the set of materials and corresponding thicknesses representing that particular position, gives maximum transmission over the user defined passbands and minimum transmission elsewhere.

(iv) *Personal Best (Pbest)*: This refers to the location with the best value of fitness function personally encountered so far by the bee. The bee constantly compares the fitness function value corresponding to the current location with that given by *Pbest* (denoted as *Pbest_value)*. If the current location is found to have a better fitness function value, *Pbest* would be replaced with this current location.

(v) *Global Best (Gbest)*: This refers to the location with the best fitness function value encountered so far by the swarm of bees. At a new position, the bee would always compare the value of fitness function with that corresponding to *Gbest* (denoted as *Gbest_value)*. If found better,then *GBest* would be replaced with the bee's current location.

5. ALGORITHM FOR THE OPTIMIZATION OF MULTI-LAYERED RADOME

The step-by-step procedure for the implementation of PSO, in the context of optimization of material layer sequence and thickness profile of an M layered radome for multi-band power transmission, is elaborately presented here. As explained in the previous section, the position of a particle corresponding to the M layered problem will have a dimension of $2M$ which includes M materials as well as M thicknesses. The various steps in the algorithm are given below.

5.1. Specification of User Defined Inputs and Definition of Solution Space

In this step, the parameters to be optimized and their respective ranges are clearly defined. For the multi-layered radome problem, material numbers corresponding to each layer and the respective thicknesses have been identified as the parameters to be optimized. The material number corresponds to the number designated to a particular material in the pre-defined material database.The required number of layers (M), number of particles (P), number of materials in the database (N), number of iterations (X), angle of incidence ($Theta$), edge frequencies corresponding to the required passbands and maximum and minimum values for the thickness of each layer have been taken as user defined inputs. The maximum and minimum values for the material number corresponding to each layer as well the maximum and minimum values for the thickness of each layer have been stored in matrices $A_{\min}$ and $A_{\max}$ respectively. The format for both the matrices are illustrated below:

$$A_{\min} = \begin{bmatrix} 1 & t_{1\,\min} \\ 2 & t_{2\,\min} \\ \vdots & \vdots \\ M & t_{M\,\min} \\ M+1 & m_{M+1\,\min} \\ M+2 & m_{M+2\,\min} \\ \vdots & \vdots \\ 2M & m_{2M\,\min} \end{bmatrix}, \quad A_{\max} = \begin{bmatrix} 1 & t_{1\,\max} \\ 2 & t_{2\,\max} \\ \vdots & \vdots \\ M & t_{M\,\max} \\ M+1 & m_{M+1\,\max} \\ M+2 & m_{M+2\,\max} \\ \vdots & \vdots \\ 2M & m_{2M\,\max} \end{bmatrix}$$

In both the matrices, the first element of each row corresponds to the dimension number. Further, the first M elements in the second column $(t_1, t_2, \ldots, t_M)$ corresponds to layer thicknesses and the remaining M elements denote the corresponding material numbers $(m_{M+1}, m_{M+2}, \ldots, m_{2M})$.

5.2. Formulation of Fitness Function

The fitness function has to be formulated appropriately to identify the quality of a position. The main objective in the present case is to identify the set of parameters that can provide maximum power transmission and minimum power reflection in the user defined passband for a comparatively high angle of incidence. At the same time, it should also ensure minimum power transmission in the stopband. The required variation in power transmission characteristics w.r.t. frequency (f) for a multi-layered radome functional over a single passband and a single stopband is shown in Fig. 2. The fitness function for achieving the characteristics as illustrated in Fig. 2 has been uniquely formulated as,

$$F = F_1 + F_2 \tag{12}$$

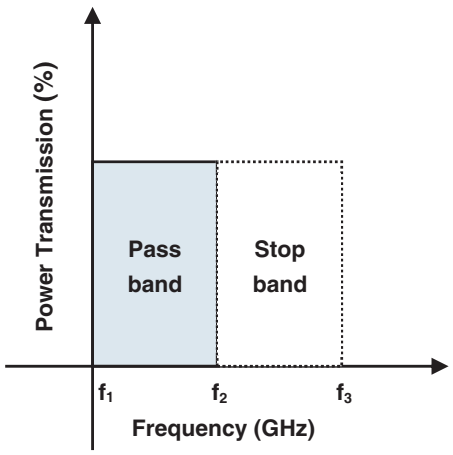

Figure 2. Desired variation in power transmission characteristics w.r.t. frequency for a multi-layered radome functional over a single passband and a single stopband.

where,

$$F_1 = \sum_{f=f_1}^{f_2} \left[\frac{1}{\widetilde{RC}_{\max}} |a|^k + w_1 \times \widetilde{TC}_{1\max} \left| \frac{1}{b} \right|^k \right] \tag{13}$$

$$F_2 = \sum_{f=f_2}^{f_3} \left[\frac{1}{\widetilde{RC}_{\max}} |a|^k + w_2 \times \widetilde{TC}_{2\max} |b|^k \right] \tag{14}$$

$$a = \widetilde{RC}_f - \widetilde{RC}_{\min} \tag{15}$$

$$b = \widetilde{TC}_f - \widetilde{TC}_{\min} \tag{16}$$

The notations $\widetilde{RC}_f$, $\widetilde{RC}_{\min}$, and $\widetilde{RC}_{\max}$ correspond to the overall recursive reflection coefficient of the multi-layered radome wall configuration at fth frequency, desired minimum value for overall recursive reflection coefficient, and permissible maximum value for overall recursive reflection coefficient, respectively. The same meaning applies to transmission coefficients as well. w_1 and w_2 denote the weight parameters. Further, (f_1, f_2), and (f_2, f_3) denote the edge frequencies corresponding to the required passband and stopband, respectively.

Here, lower the value of fitness function, better will be the position as it would yield minimum reflection along with maximum transmission in the desired passband and reverse characteristics in the stopband. The constant k has been introduced in the fitness function to move the focus of optimization to those frequencies with higher reflection coefficient and lower transmission coefficient in the passband and vice versa. In the current problem, k has been assigned a value of 2. As the number of passbands and stopbands increase, the number of terms in F have to be increased as well in order to account for the power characteristics in each band.

5.3. Initialization of Random Positions and Velocities

The random locations from which particles start moving and the random velocities with which they move have to be initialized in this step. The matrix $(T)_{J\times I}$ containing the initial positions of all the particles can be written as,

$$T = \begin{bmatrix} 1 & t_{11} & t_{12} & t_{13} & \dots & t_{1M} & m_{11} & m_{12} & m_{13} & \dots & m_{1M} \\ 2 & t_{21} & t_{22} & t_{23} & \dots & t_{2M} & m_{21} & m_{22} & m_{23} & \dots & m_{2M} \\ 3 & t_{31} & t_{32} & t_{33} & \dots & t_{3M} & m_{31} & m_{32} & m_{33} & \dots & m_{3M} \\ \vdots & \vdots & \vdots & \vdots & \dots & \vdots & \vdots & \vdots & \vdots & \dots & \vdots \\ \vdots & \vdots & \vdots & \vdots & \dots & \vdots & \vdots & \vdots & \vdots & \dots & \vdots \\ P & t_{P1} & t_{P2} & t_{P3} & \dots & t_{PM} & m_{P1} & m_{P2} & m_{P3} & \dots & m_{PM} \end{bmatrix}$$

where P denotes the number of particles.

The first element in a particular row denotes the particle number, and the following elements correspond to the position of the particle. In the present problem, position is composed of the thicknesses of different layers followed by the respective material numbers. The matrix containing the initial velocities of the parameters can also be represented in a similar manner.

5.4. Setting the Trajectory of Particles in the Solution Space

Once the initial positions and velocities for all the particles are randomly assigned, they have to be moved through the solution space. The steps to be followed for setting the trajectory of each particle are given below:

***Step* (5.4)-1:** Here, the fitness function corresponding to the current position of a particle has to be computed and then compared with its *Pbest_value* and *Gbest_value*. If the value of fitness function at the current location is better than *Pbest_value* and *Gbest_value*, the appropriate positions are replaced with the current position.

***Step* (5.4)-2:** In this step, the velocities of all particles have to be modified w.r.t. *Pbest* and *Gbest*. The generalized equations for updating the velocity of each dimension can be expressed as [17],

$$VEL_{iD}^{j} = q \times VEL_{iD}^{j-1} + k_1 \times rand1_{iD}^{j}() \times \left(Pbest_{iD}^{j-1} - T_{iD}^{j-1}\right) + k_2 \times rand2_{iD}^{j-1}() \times \left(Gbest_{D}^{j-1} - T_{iD}^{j-1}\right) \quad (17)$$

$$VEL_{iD}^{j} = \min\left(VEL_{\max}^{D}, \max\left(VEL_{\min}^{D}, VEL_{iD}^{j}\right)\right) \quad (18)$$

where i, j, VEL_{iD}, T_{iD}, and q denote particle number, iteration number, velocity of the particle in the Dth dimension, particle's co-ordinate in the Dth dimension, and inertial weight respectively. k_1 and k_2 denote the acceleration constants which determine the relative pull of *Gbest* and *Pbest*. Further, *rand*1( ) and *rand*2( ) are random number functions which generate uniform random numbers between 0 and 1.

***Step* (5.4)-3:** Once the new velocities are found, the particles have to be moved with these modified velocities. The next position can be written as,

$$T_{iD}^{j} = T_{iD}^{j-1} + VEL_{iD}^{j} \quad (19)$$

In order to confine the particles within the solution space, the modified positions have to be constantly checked. If solution is found out of bounds, appropriate boundary conditions like absorbing walls, reflecting walls, invisible walls etc. have to be applied [27].

5.5.

Once steps (5.1) to (5.4) are completed for all the particles, the procedure has to be repeated from Step (5.4) until a particular condition is satisfied or when pre-defined number of iterations are completed. A comprehensive flow chart for the developed algorithm is shown in Fig. 3.

6. PREPARATION OF SILICON NITRIDE BASED MATERIAL DATABASE

Silicon nitride is a prospective broadband radome material especially suitable for high speed applications due to its superior temperature resistance and attractive mechanical properties. The multi-band radomes considered in this paper have been realized using a number of layers of Si_3N_4 with varying porosity. The constitutive parameters corresponding to mth layer, made up of Si_3N_4 with a porosity of P (in %), can be predicted [28] as,

$$\varepsilon_{rm} = (1 - g_m) + g_m \varepsilon_{r_{\max}}(1 - j \tan\delta_{\max}) = \varepsilon_{rm_{real}} + j\varepsilon_{rm_{imag}}; \quad m = 1, 2, \ldots, M \quad (20)$$

$$\tan\delta_m = \frac{\varepsilon_{rm_{imag}}}{\varepsilon_{rm_{real}}} \quad (21)$$

$$P\,(in\ \%) = (1 - g_m) \times 100 \quad (22)$$

where $\varepsilon_{r_{\max}} = \max\{\varepsilon_{rm}\} = 7$; $\tan\delta_{\max} = \max\{\tan\delta_m\} = 0.006$, g_m is the relative volume of space occupied by the dielectric in the mth layer.

In accordance with Equations (20) and (21), a material database containing several variants of Si_3N_4 with different porosities has been created, as shown in Table 1.

7. RESULTS AND DISCUSSION

The algorithm for the optimal design of multi-band radomes using PSO has been implemented in FORTRAN. A discrete subroutine has been developed for the computation of overall recursive reflection and transmission coefficients of multi-layered radomes, and the results obtained have been validated by comparing with those obtained using full wave simulation software (FEKO). The power characteristics of a two-layered dielectric media (Layer#1: $\varepsilon_r = 2.2$, $\tan\delta = 0.002$, thickness = 6.44 mm; Layer#2: $\varepsilon_r = 7$, $\tan\delta = 0.006$, thickness = 0.62 mm) computed using the developed subroutine as well as FEKO are presented in Fig. 4. It is clear from the plots that the results obtained using developed subroutine

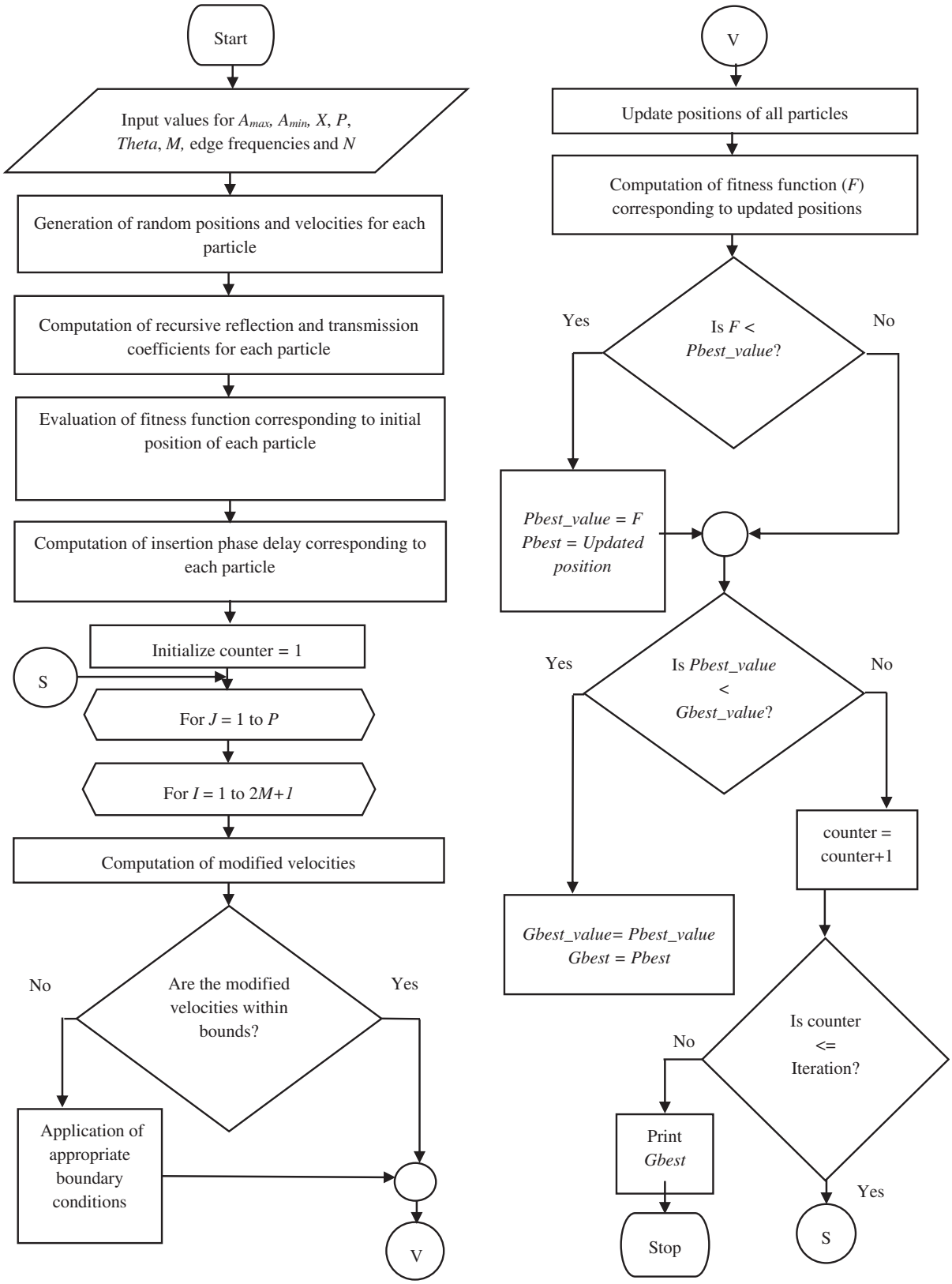

Figure 3. Flowchart for the optimal design of multi-layered radome using PSO.

Table 1. Material database based on Si_3N_4 with different porosities.

Material Number	Porosity of Si_3N_4 (in %)	ε_r	tanδ
1	2	7	0.00600
2	5	6.7	0.00595
3	10	6.4	0.00591
4	15	6.1	0.00585
5	20	5.8	0.00580
6	25	5.5	0.00572
7	30	5.2	0.00565
8	35	4.9	0.00560
9	40	4.6	0.00547
10	45	4.3	0.00537
11	50	4	0.00525
12	55	3.7	0.00512
13	60	3.4	0.00490
14	65	3.1	0.00474
15	70	2.8	0.00450
16	75	2.5	0.00420
17	80	2.2	0.00382
18	85	1.9	0.00332
19	90	1.6	0.00263
20	95	1.3	0.00160

are in good agreement with those obtained using FEKO thereby establishing its authenticity. Once validation of the developed subroutine is obtained, the subroutine has been integrated into the PSO algorithm for computation of fitness function as expressed in Eq. (12).

Further, the performance of the indigenously developed code has been evaluated by carrying out the design of multi-band radomes based on silicon nitride (Si_3N_4). Based on the material database as presented in Table 1, the indigenously developed PSO based code has been used for determining the optimal material layer sequence and thickness profile of two five layered radomes with passbands as mentioned below:

Radome#1: Passband-1: 5 GHz to 10 GHz;
Passband-2: 15 GHz to 20 GHz.

Radome#2: Passband-1: 10 GHz to 15 GHz;
Passband-2: 20 GHz to 25 GHz.

The number of particles and number of iterations have been fixed as 120 and 50. Other parameters have been chosen as $\widetilde{RC}_{\min} = 0.2236$, $\widetilde{RC}_{\max} = 0.31622$, $\widetilde{TC}_{\min} = 0.31622$, $\widetilde{TC}_{1\max} = 0.99949$, $\widetilde{TC}_{2\max} = 0.4472$, $w_1 = 100$, $w_2 = 200$, $q = 0.9$, $k_1 = k_2 = 1.49$. All the parameters have been finalized after performing extensive convergence studies. The maximum and minimum values of thickness corresponding to each constituent layer have been taken as 0.1 mm and 10 mm respectively. On fixing all the required parameters, the PSO based code has been executed assuming a TE polarized plane wave incident at an angle of 45° on the planar radome wall configuration. The optimized material layer sequence and thickness profile suggested by the indigenously developed code for Radome#1 and Radome#2 are given in Table 2 and Table 3, respectively.

A representative schematic diagram for the five-layered radome wall configuration is shown in Fig. 5. The frequency dependent power transmission characteristics for both the radomes are presented

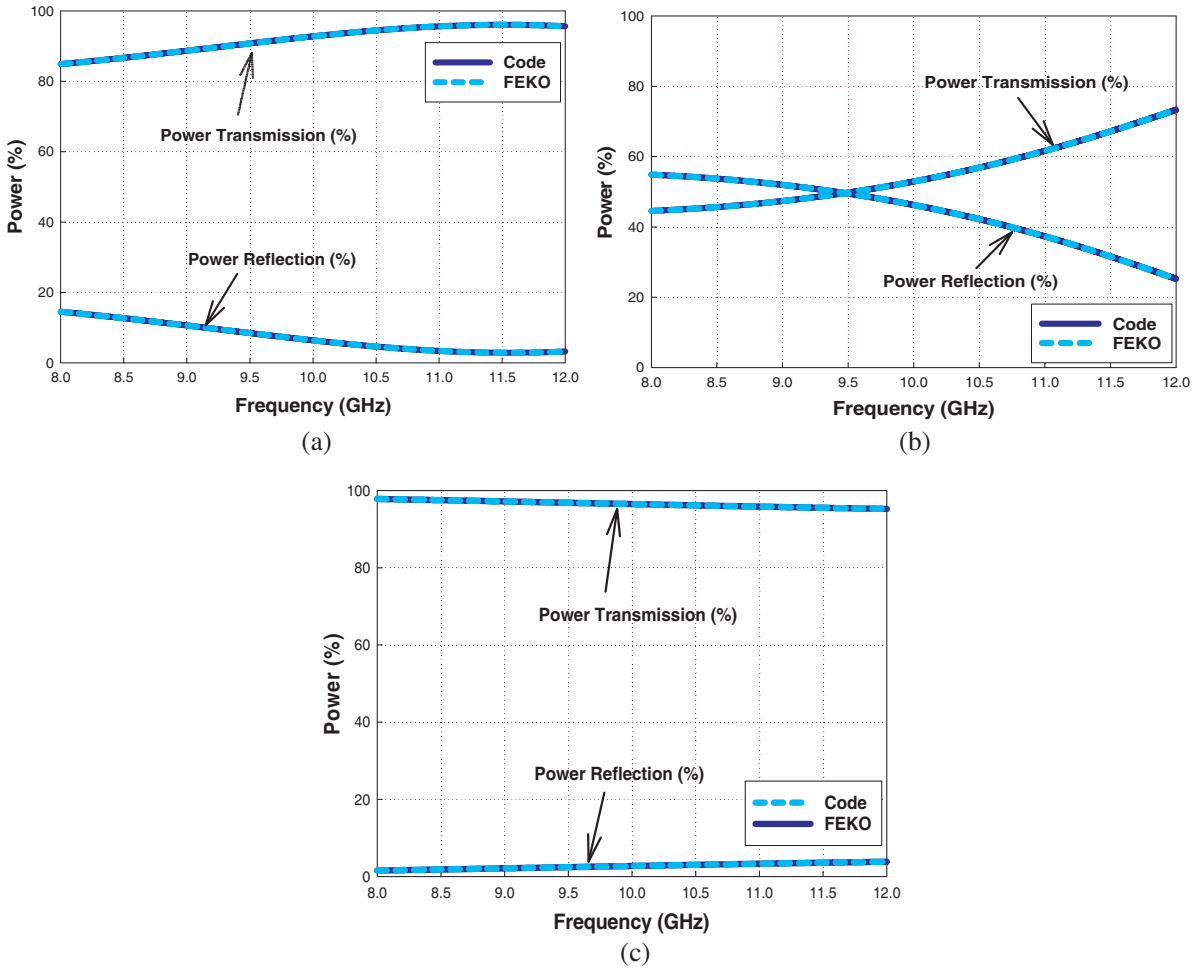

Figure 4. Comparison of power characteristics of two layered dielectric media computed using developed subroutine and FEKO. (a) $\theta = 0°$ (normal incidence), (b) $\theta = 60°$ (TE polarization), (c) $\theta = 60°$ (TM polarization).

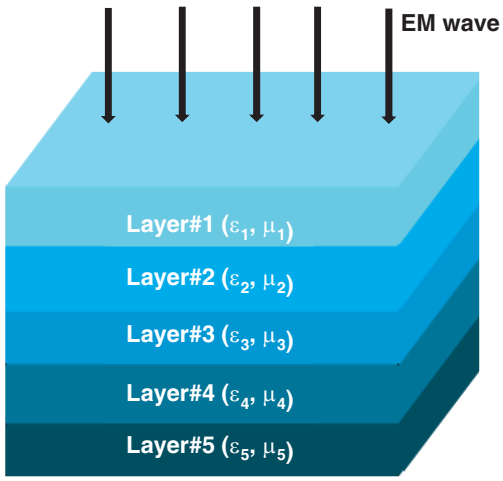

Figure 5. Schematic diagram of five-layered radome wall configuration.

Table 2. Configuration of Radome#1.

Layer	Porosity of Si_3N_4 (in %)	ε_r	tanδ	Thickness (mm)
1	65	3.1	0.005108	4.628
2	70	2.8	0.0045	3.285
3	2	7	0.006	1.848
4	75	2.5	0.0042	4.843
5	70	2.8	0.0045	3.627
Total thickness				18.231

Table 3. Configuration of Radome#2.

Layer	Porosity of Si_3N_4 (in %)	ε_r	tanδ	Thickness (mm)
1	95	1.3	0.0016	3.496
2	35	4.9	0.0056	2.053
3	20	5.8	0.0058	3.442
4	90	1.6	0.0026	5.275
5	60	3.4	0.0049	7.358
Total thickness				21.624

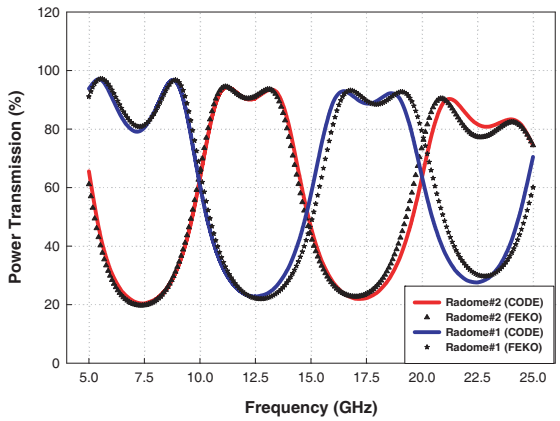

Figure 6. Variation in power transmission characteristics of optimized radome wall configurations w.r.t. frequency.

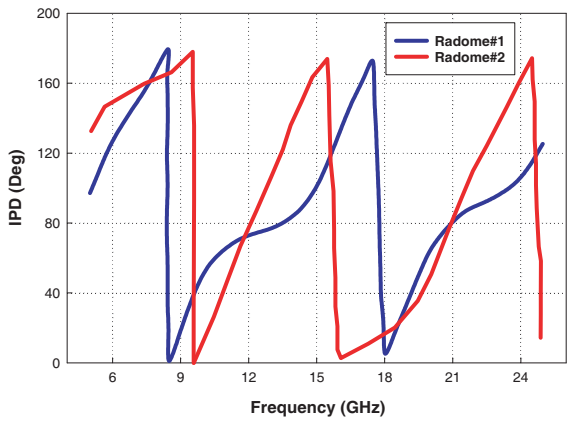

Figure 7. Variation in IPD of optimized radome wall configurations w.r.t. frequency.

in Fig. 6. The computed results have been validated with those of FEKO. It is clearly evident that the percentage of power transmitted is above 80% in the passbands for both the optimized radome wall configurations thereby establishing the accuracy of the uniquely formulated fitness function. Further, as per the reciprocity theorem for stratified media [29–31], the magnitude of transmission coefficient will remain the same when the plane wave is incident on Layer 1 or Layer 5. Hence, the power transmission characteristics of both the radomes will remain unchanged irrespective of whether the antenna is in transmitting mode or receiving mode. Furthermore, in view of structural rigidity, Layer 1 (65% Porosity) of Radome#1 and Layer 5 (60% Porosity) of Radome#2 can be considered as outermost layers. The variation in insertion phase delay (IPD) w.r.t. frequency for Radome#1 and Radome#2 is shown in Fig. 7. The plots clearly indicate that IPD is well within the stipulated limits.

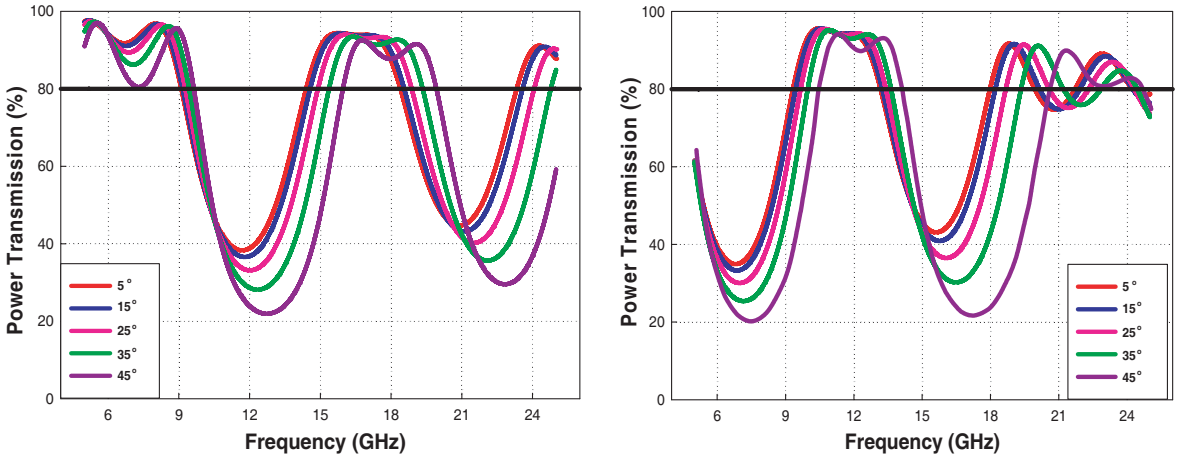

Figure 8. Variation in the power transmission characteristics w.r.t. frequency for different incident angles for TE polarization. (a) Radome#1, (b) Radome#2.

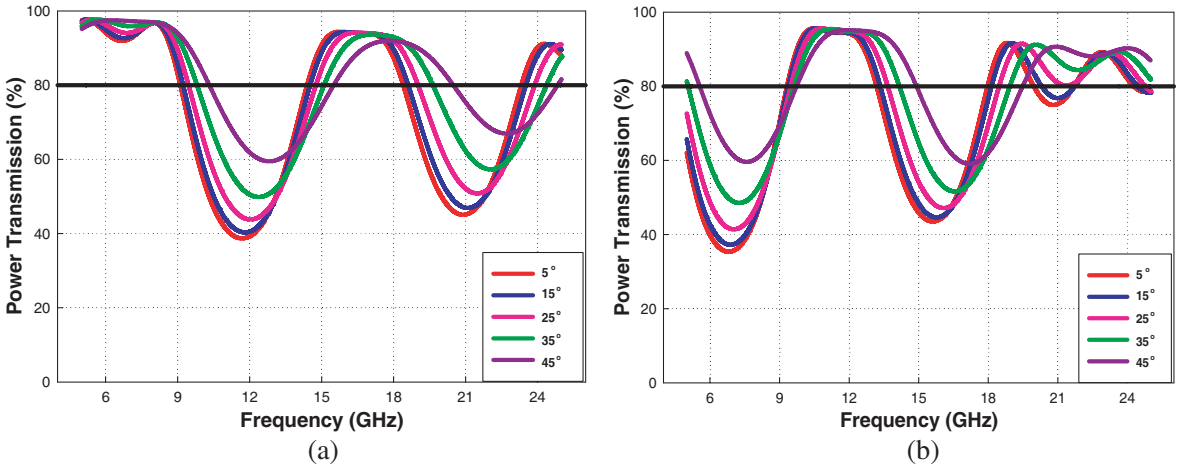

Figure 9. Variation in the power transmission characteristics w.r.t. frequency for different incident angles for TM polarization. (a) Radome#1, (b) Radome#2.

The variation in power transmission characteristics of both the optimized radome wall configurations w.r.t. frequency at different incident angles for TE polarization and TM polarization are shown in Fig. 8 and Fig. 9, respectively. It is clearly evident from the plots that the performance is well within the desirable limits for a wide range of incident angles thereby establishing the efficiency of the algorithm.

In order to assess the computational efficiency of the indigenously developed PSO based algorithm, the total simulation time taken has been compared with that taken by the PSO based optimization utility available in FEKO. However, FEKO doesn't have the feature for automatic selection of suitable materials for constituent layers. Therefore, different material combinations have to be selected manually and their thicknesses have to be optimized separately in FEKO. In the present case, with a pre-defined database containing 20 materials, the total number of material combinations possible for a five-layered radome wall configuration can be calculated as,

$$\textit{Total number of possible material combinations} = 20^5$$

This implies that the PSO utility in FEKO has to be executed 20^5 times for all these possible combinations in order to estimate the corresponding optimized thickness profiles for achieving user

defined performance. On completion of all these simulations, the resulting optimized models have to be compared to conclude upon the final optimized five-layered radome wall configuration. The estimated simulation time in FEKO, for performing the PSO based optimization of thickness profile of a five layered radome over the frequency regime 5 GHz to 25 GHz (total number of frequency points = 232; step size for thickness of each layer = 0.1 mm) is 3 hours. The simulation has been performed in Dell precision tower 7810 workstation (Two Intel Xeon CPUs E5-2650 v4 @ 2.20 GHz; RAM: 256 GB). Therefore, the total simulation time for completing the optimization of a five layered radome wall configuration in FEKO would be $20^5 \times 3 = 9600000$ hours. i.e., approximately 400000 days. Instead, the indigenously developed PSO based code took less than 10 minutes for the complete procedure, thereby proving its computational efficiency.

8. CONCLUSION

Multi-layered radome wall configurations are preferred candidates for aerospace applications due to their superior performance w.r.t. bandwidth and structural rigidity. However, the optimization of layer sequence and thickness profile is a computationally intensive task especially when a huge database of potential materials is available. In this regard, an efficient particle swarm optimization (PSO) based algorithm for material selection as well as thickness optimization of multi-layered planar radomes for multiband applications has been introduced. The fitness function has been uniquely formulated to identify the set of parameters that can provide maximum power transmission and minimum power reflection in the user defined passbands for a comparatively high angle of incidence. Further, a full wave formulation has been used for the computation of overall reflection/transmission coefficients of the multi-layered radome in order to improve the accuracy of the optimization algorithm. The case study using a material database containing 20 silicon nitride based materials clearly established the efficiency of the algorithm by achieving above 80% power transmission in the user defined passbands. Further, as per the reciprocity theorem for stratified media, the power transmission characteristics of the proposed radomes will remain unchanged irrespective of whether the antenna is in transmitting mode or receiving mode. The superior computational efficiency of the developed code over the PSO based optimization algorithm in FEKO has also been proved. Therefore, the indigenously developed algorithm presents an efficient design methodology for the realization of multiband radomes that can be used in autonomous radar systems operating at different frequency bands.

REFERENCES

1. Zhou, L., Y. Pei, and D. Fang, "Dual-band A-sandwich radome design for airborne applications," *IEEE Antennas and Wireless Propagation Letters*, Vol. 15, 218–221, 2016.
2. Zhou, L., Y. Pei, R. Zhang, and D. Fang, "Method for design of dual-band flat radome wall structure," *American Institute of Aeronautics and Astronautics Journal*, Vol. 51, No. 12, 2819–2822, 2013.
3. Zhou, L. C., Y. M. Pei, R. B. Zhang, and D. N. Fang, "A multilayer radome wall structure with passbands having odd times of selected central frequencies," *Journal of Electromagnetic Waves and Applications*, Vol. 26, No. 16, 2154–2164, 2012.
4. Zhou, L., Y. Pei, R. Zhang, and D. Fang, "Optimal design for high-temperature broadband radome wall with symmetrical graded porous structure," *Progress In Electromagnetics Research*, Vol. 127, 1–14, 2012.
5. Pei, Y., A. Zeng, L. Zhou, R. Zhang, and K. Xu, "Electromagnetic optimal design for dual-band radome wall with alternating layers of staggered composite and Kagome lattice structure," *Progress In Electromagnetics Research*, Vol. 122, 437–452, 2012.
6. Chen, F., Q. Shen, and L. Zhang, "Electromagnetic optimal design and preparation of broadband ceramic radome material with graded porous structure," *Progress In Electromagnetics Research*, Vol. 105, 445–461, 2010.

7. Vinisha, C. V., P. S. M. Yazeen, V. Joy, R. U. Nair, and P. Mahima, "Multi-layered graded porous radome design for dual-band airborne radar applications," *Electronics Letters*, Vol. 53, No. 3, 189–191, Feb. 2017.
8. Xu, G., S. V. Hum, and G. V. Eleftheriades, "A technique for designing multilayer multistopband frequency selective surfaces," *IEEE Transactions on Antennas and Propagation*, Vol. 66, No. 2, 780–789, Feb. 2018.
9. Xu, G., S. V. Hum, and G. V. Eleftheriades, "Systematic design ofsingle-layer multi-stop-band frequency selective surfaces," *Proc. IEEE Antennas Propag. Soc. Int. Symp. (APSURSI)*, 261–262, Jul. 2017.
10. Gao, M., S. M. A. M. H. Abadi, and N. Behdad, "A dual-band inductively coupled miniaturized-element frequency selective surfacewith higher order bandpass response," *IEEE Transactions on Antennas and Propagation*, Vol. 64, No. 8, 3729–3734, Aug. 2016.
11. Liu, N., X. Sheng, C. Zhang, and D. Guo, "Design of dual-band composite radome wall with high angular stability using frequency selective surface," *IEEE Access*, Vol. 7, 123393–123401, 2019, doi: 10.1109/ACCESS.2019.2937977.
12. Yan, M., J. Wang, H. Ma, M. Feng, Y. Pang, S. Qu, J. Zhang, and L. Zheng, "A tri-band, highly selective, bandpass FSS using cascaded multilayer loop arrays," *IEEE Transactions on Antennas and Propagation*, Vol. 64, No. 5, 2046–2049, May 2016.
13. Ichikawa, K., *Functionally Graded Materials in the 21st Century: A Workshop on Trends and Forecasts*, 235, Springer, New York, USA, ISBN 978-1-4615-4373-2, 2001.
14. Mahamood, R. M. and E. T. Akinlabi, *Functionally Graded Materials*, 103, Springer, New York, USA, ISBN 978-3-319-53756-6, 2017.
15. Kennedy, J. and W. M. Spears, "Matching algorithms to problems: An experimental test of the particle swarm and some genetic algorithms on the multimodal problem generator," *1998 IEEE International Conference on Evolutionary Computation Proceedings*, 78–83, Anchorage, AK, USA, 1998.
16. Sivakoti, K. K., M. Basava, R. V. Balaga, and B. M. Sannidhi, "Design optimization of radar absorbing materials using particle swarm optimization," *International Journal of Applied Metaheuristic Computing*, Vol. 8, No. 4, 113–132, 2017.
17. Roy, S., S. D. Roy, J. Tewary, A. Mahanti, and G. K. Mahanti, "Particle swarm optimization for optimal design of broadband multilayer microwave absorber for wide angle of incidence," *Progress In Electromagnetics Research B*, Vol. 62, 121–135, 2015.
18. Chiba, H., K. Nishizawa, H. Miyashita, and Y. Konishi, "Optimal design of broadband radome using particle swarm optimization," *IEEJ Transactions on Electrical and Electronic Engineering*, Vol. 7, No. 4, 343–349, 2012.
19. Lee, K.-W., I.-P. Hong, B.-J. Park, Y.-C. Chung, and J.-G. Yook, "Design of multilayer radome with particle swarm optimization," *The Journal of Korean Institute of Electromagnetic Engineering and Science*, Vol. 21, No. 7, 744–751, 2010, doi: 10.5515/KJKIEES.2010.21.7.744.
20. Nguyen, T. K., I. G. Lee, O. Kwon, Y. J. Kim, and I. P. Hong, "Metaheuristic optimization techniques for an electromagnetic multilayer radome design," *Journal of Electromagnetic Engineering and Science*, Vol. 19, 31–36, 2019, doi:10.26866/JEES.2019.19.1.31.
21. Chew, W. C., *Waves and Fields in Inhomogeneous Media*, 45–53, IEEE Press, New York, ISBN: 978-0-780-34749-6, 1995.
22. Balanis, C. A, *Advanced Engineering Electromagnetics*, 1040, John Wiley & Sons, USA, ISBN: 978-0-470-58948-9, 2012.
23. Pozar, D. M., *Microwave Engineering*, 39–43, John Wiley & Sons, USA, ISBN 978-0-470-63155-3, 1998.
24. Nair, R. U., S. Shashidhara, and R. M. Jha, "Novel inhomogeneous planar layer radome design for airborne applications," *IEEE Antennas and Wireless Propagation Letters*, Vol. 11, 854–856, 2012.
25. Kozakoff, D. J., *Analysis of Radome-enclosed Antennas*, 317, Artech House, USA, ISBN: 97815969344298, 2009.

26. Rudge, A. W., K. Milne, A. D. Olver, and P. Knight, *The Handbook of Antenna Design*, 462–477, IET, London, ISBN o-906042-82-6, 1983.
27. Robinson, J. and Y. Rahmat-Samii, "Particle swarm optimization in electromagnetics," *IEEE Transactions on Antennas and Propagation*, Vol. 52, No. 2, 397–407, Feb. 2004.
28. Zhang, Y., Z. Zhao, Z. P. Nie, and Q. H. Liu, "Optimization of graded materials for broadband radome wall with DRR control using a hybrid method," *Progress In Electromagnetics Research M*, Vol. 43, 193–201, 2015.
29. Potton, R. J., "Reciprocity in optics," *Reports on Progress in Physics*, No. 67, 717–754, 2004, doi: 10.1088/0034-4885/67/5/R03.
30. Vigoureux, J. M. and R. Giust, "Explicit Stokes reciprocity relations for plane stratified media," *Optics Communications*, No. 176, 1–8, 2000.
31. Carminati, R. and M. N. Vesperinas, "Reciprocity of evanescent electromagnetic waves," *Journal of the Optical Society of America A*, Vol. 15, No. 3, 706–712, 1998.